Check for updates

# Adsorption and diffusion of H$_2$ and CO on UiO-66: A Monte Carlo simulation study

Negin Davoodian * [iD] and Zahra Khoshbin [iD]

*Department of Chemistry, Faculty of Science, Ferdowsi University of Mashhad, Mashhad 91775-1436, Iran*
davoodiannegin@gmail.com (N.D.), zahra.khoshbin@mail.um.ac.ir (Z.K.)

* Corresponding author at: Department of Chemistry, Faculty of Science, Ferdowsi University of Mashhad, Mashhad 91775-1436, Iran.
 e-mail: davoodiannegin@gmail.com (N. Davoodian).

## RESEARCH ARTICLE

## ABSTRACT

Metal-organic frameworks (MOFs) are a new class of nanoporous materials that have attracted much attention for the adsorption of small molecules, due to the large size of the cavities. In this study, we investigate the adsorption and diffusion of hydrogen (H$_2$) and carbon monoxide (CO) guest molecules to the UiO-66 framework, as one of the most widely used MOFs, by using Monte Carlo simulation method. The results prove that an increment in the temperature decreases the amount of the adsorbed H$_2$ and CO on the UiO-66 framework. While an enhancement of the pressure increases the amount of the adsorbed H$_2$ and CO on the UiO-66 framework. Besides, the adsorption of H$_2$ and CO on UiO-66 is the type I isotherm. The calculated isosteric heat for CO/UiO-66 is slightly higher than that of H$_2$/UiO-66. The means of square displacement (MSD) value is less for CO molecule; hence, the movement of the guest molecule within the host cavity slows down and the guest molecule travels a shorter distance over a period of time. The guest molecule with higher molecular mass possesses less mobility, and therefore, it will have less permeability.

## 1. Introduction

Recent years have witnessed the growing development in the renewable energy, due to the finite sources of the fossil fuels and severe climate changes caused by their overuse [1]. Among the available devices for producing the renewable energy, the fuel cell systems have attracted a great attention because of some significant advantages, such as high thermodynamic efficiency, low operational cost, and scalability [2,3]. However, these systems are hydrogen consumer devices; hence, hydrogen can be a utile source for the energy production [3]. Carbon monoxide, as one of the small components of the air layer, can be a result of the natural processes and human activities. Currently, the increment of the CO concentration near urban areas has become one of the major environmental concerns. In recent decades, the numerous efforts have been made to eliminate CO with high efficiency and economically, even in a small percentage in the converted gases. Adsorption is one of the most common methods for removing CO molecule [4].

The generation and storage of H$_2$ and CO are the principal issues that should be considered in the field of fuel cell systems. Hence, it is important for researchers to design and introduce the cost-effective and secure methods for the H$_2$ and CO storage.

Adsorbents are the promising tools for this purpose, due to the significant features, including high storage capacity, light weighting, regenerability, etc. [5-7]. Up to now, the different H$_2$ storage materials are introduced extensively. The metal-organic frameworks are one of the most applicable substances, especially for their particular porosity and high surface area [8]. The MOFs containing zirconium (Zr) atom are applied greatly as the efficient adsorbents for the H$_2$ storage [9]. UiO-66, a Zr-based MOF, is considered as the efficient H$_2$ and CO adsorbent [10]. Some structural parameters that have a significant influence on the adsorbent's efficiency are surface area, number of active sites, type of functional groups, internal layers, and also, pore shape and size [11,12].

There are different studies clarifying that the preparation conditions possess impressive effects on the adsorbent functionality [13]. For example, Yang *et al.* [14] studied the influence of the zeolite template and nitrogen doping on the ability of the zeolite template carbon materials for the H$_2$ storage. They found that the H$_2$ uptake was dependent on the surface, and therefore, the choice of the zeolite template and carbon source possessed a critical role to achieve the highest H$_2$ storage. Besides, Xie *et al.* [15] investigated the effect of the preparation conditions of the carbon adsorbents on the H$_2$ adsorption capacity.
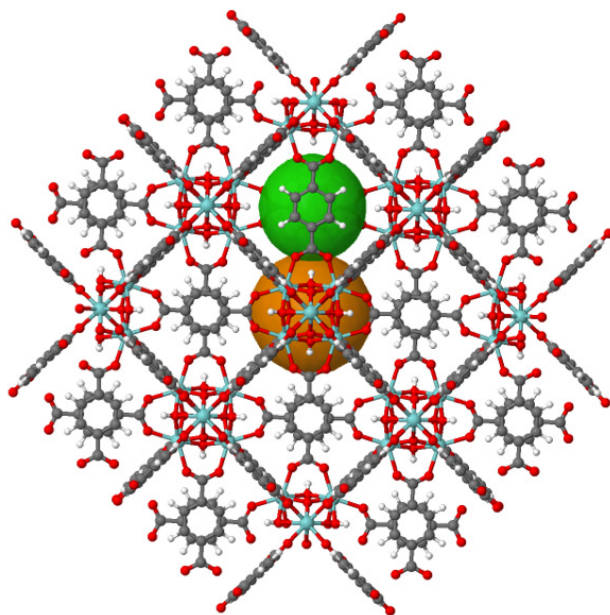
**Figure 1.** Crystal structure of cell (2×2×2) in the UiO-66 framework (color elements: Zirconium: green, Oxygen: red, Carbon: gray, and Hydrogen: white).

The different preparation conditions induced the changes in the structure of the adsorbents that influenced their storage capacity. Many studies by using the computational methods highlight the effect of the adsorbent structure on the adsorption process. Jeffery *et al.* [16] studied the adsorption of water onto the MOF-5 by using a molecular dynamics (MD) simulation method that demonstrated a new insight into the mechanism of MOF-5 displacement in contact with water. Since the bond between zinc ions and oxygen atoms in the MOF-5 was weak, the attack was allowed by water molecules.

One of the most widely applied approaches to investigate the gas adsorption process is the Grand Canonical Monte Carlo (GCMC) method. Zheng *et al.* [17] investigated the $H_2$ adsorption on MOF-505. The results proved that the ligand expansion, especially through the alkyne bonds, was an effective way to enhance the MOF surface area and pore volume that efficiently increased the gas uptake. Stern *et al.* [18] studied the $H_2$ adsorption on a new MOF by Monte Carlo simulation method. The simulation results illustrated that MOF with a porous structure and relatively small channels induced a high $H_2$ adsorption capacity by strengthening the $H_2$-MOF interactions. The $H_2$ interaction with MOF was carried out through the general principles of the potential energy distribution: Van der Waals polarization and induction. In the previous experimental studies, the role of the polarization agents was not considered significantly. However, MD simulation studies displayed the adsorption of a large number of dipolar $H_2$ through the effect of the agents on the MOFs [19]. Accurate laboratory measurement of gas uptake and diffusion in a MOF is difficult, due to the various constraints, such as the presence of solvent in the structure and the incomplete exit of solvent. In contrast, MD simulation provides a wide range of dynamic and thermodynamic properties of MOF [20].

In this study, a systematic simulation study is achieved on the adsorption of $H_2$ and CO in the zirconium metal organic (UiO-66) framework. We utilize UiO-66 framework as an adsorbent and then study the adsorption of $H_2$ and CO on UiO-66 at the different temperatures. The main aim of the study is to determine the best adsorption rate of $H_2$ and CO on UiO-66. Finally, the relationship is obtained between the diffusivity, pressure, temperature, and UiO-66 pore size.

## 2. Experimental

### 2.1. Simulation method

The Materials Studio software (BIOVIA, San Diego, CA, USA) [21] was used for the molecular imitation of the adsorption and diffusion of $H_2$ and CO in UiO-66. The crystallographic information file (CIF) of the UiO-66 structure was available in the Crystallographic Cambridge Data Centre (CCDC) (Figure 1), used for all the simulations without any modification [22]. The unit cell of the cubic framework possessed 456 atoms with the dimensions of 20.9784 Å. Besides, the spatial group of the cube cell was considered $Fm\overline{3}m$ [23].

### 2.2. Isotherm and diffusivity calculations

Monte Carlo simulation and adsorption module were used to predict the $H_2$ and CO adsorption in Material Studio software. Metropolis sampling is connected to GCMC and was used to predict the adsorption isotherms of UiO-66. In addition, all the simulations were done inside a 2×2×2-unit cell box with a cut-off radius of 12.5 Å. The Lennard-Jones potential parameters and universal force field (UFF) were used in the simulations. The electrostatic interactions were calculated using the Ewald summation method. The atomic bond radius, van der Waals parameters, hybridization angles, and the set of core loads were also calculated by the universal force field. The diffusion of CO and $H_2$ in UiO-66 was studied at 298 K. The self-diffusion coefficient (Ds) was calculated by means of square displacement method [24].

## 3. Results and discussions

### 3.1. Temperature and pressure effect on $H_2$ and CO isotherms

Diagrams of the adsorption isotherms for $H_2$ and CO adsorbed on UiO-66 at the different temperatures, are shown in Figure 2. Based on Figure 2, the increment in the temperature decreases the amount of the adsorbed $H_2$ and CO on the UiO-66 framework, illustrating that the absorption process is completely spontaneous.
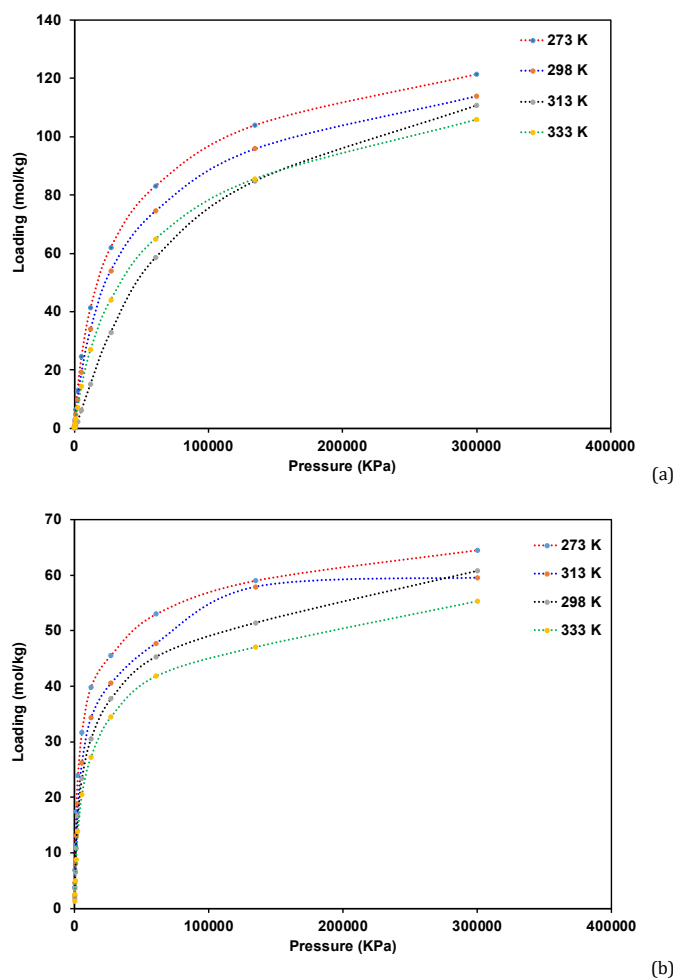
(a)



(b)

**Figure 2.** The $H_2$ adsorption isotherm (a) and CO adsorption isotherm (b) on the UiO-66 framework.

The change in the Gibbs free energies is obtained the negative value ($\Delta G < 0$); because the absorbed molecules lose their degrees of freedom for the transmission when they reach the suitable level of the adsorption. Similarly, the entropy changes are obtained the negative values ($\Delta S < 0$) during the absorption process. Therefore, the enthalpy changes ($\Delta H$) must be negative enough that the $\Delta G$ value becomes negative according to $\Delta G = \Delta H - T\Delta S < 0$. Hence, the adsorption process is exothermic, and increasing the temperature decreases the adsorption of $H_2$ and CO. Besides, the increment of the pressure enhances the amount of the adsorbed $H_2$ and CO on UiO-66 framework. The obtained adsorption isotherms for $H_2$ and CO in the UiO-66 structure are classified as the type I isotherm. Hence, it can be assumed that the porosity of the framework cavities is mainly micro-cavities. The obtained results are in consistent with the previous studies [25].

### 3.2. $H_2$ and CO adsorption on UiO-66 framework

Figure 2 illustrates the co-occurrence of the $H_2$ and CO uptake on UiO-66 by using Monte Carlo simulation at different temperatures including 273, 298, 313, and 333 K and the pressure range of 100-300000 kPa (1-3000 bar). Figure 2 depicts that the adsorption of $H_2$ and CO on UiO-66 is a type I isotherm, which is initially rapid and increases after the saturation at the pressures above 0.5 bar. The absorption of CO on UiO-66 is increased significantly at 298 K and 1300 bar in comparison with the other temperatures (Figure 2b). The main reason for the phenomenon is the increase of the Van der Waals

and electrostatic interactions, as well as the formation of the intermolecular hydrogen bonds in the UiO-66 framework.

### 3.3. Adsorption sites of $H_2$ and CO on UiO-66 framework

To identify the preferred adsorption sites of $H_2$ and CO on the UiO-66 framework, the probability density of the adsorbed molecule was obtained by using Monte Carlo simulation in the large band tuned at the different temperatures and a pressure range of 1-3000 bar. The results are indicated in Figure 3, highlighting that the volume of the UiO-66 structure remains constant at the temperatures. A comparison between the probability density of $H_2$ and CO shows that it is higher for $H_2$ (Figure 3). The higher electronegativity of $H_2$ induces its more attachment to the oxygen atoms of the UiO-66 structure, thereby increasing the electric charge of the atom. The adsorbed $H_2$ also affects the volume of the UiO-66 structure, due to its location in the space charge density.

### 3.4. Isosteric heats of adsorption

The adsorption isosteric heat was calculated by using the Equation (1).

$$q^{st} = - R \left[ \frac{\partial (lnP)}{\partial (1/T)} \right]_{loading} \tag{1}$$

in which $q^{st}$, R, P, and T are the isosteric heat of adsorption, fixed gases, pressure, and average temperature, respectively.
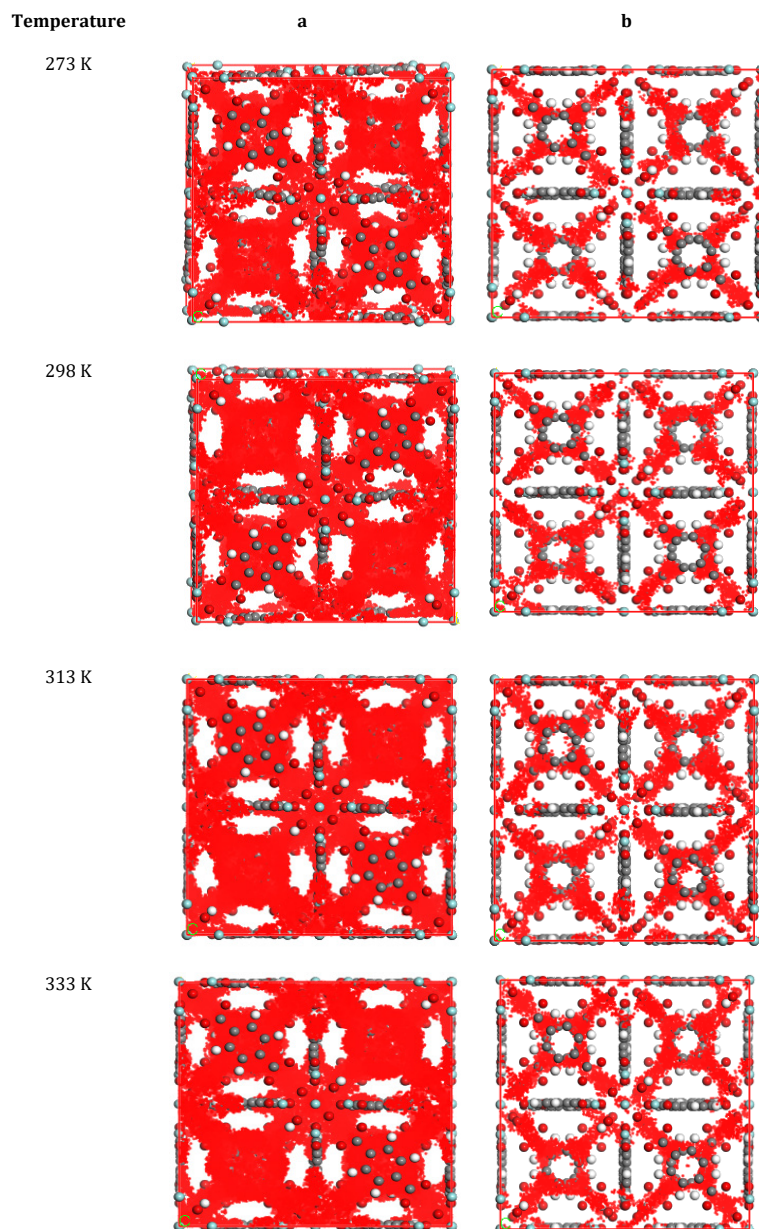
**Figure 3.** The probability density of the adsorbed $H_2$ (a) and CO (b) on the UiO-66 framework.

Figure 4 displays the isostatic heat of $H_2$ and CO on UiO-66 at the different temperatures. According to Figure 4, the isostatic heat of $H_2$ and CO is constant in the studied pressure range (1-1000 bar). The fluctuation of the absorption heat through loading is a clear indicator for the presence of the active sites with the different powers on the surface. The increment of the loading induces the full monolayer coating; then, the adsorption-adsorption (A-A) interactions are developed that result in an enhancement of the isosteric heat. The results demonstrate that the heat of the CO uptake in UiO-66 is equal to 4.2 (Table 1). The isosteric heat in CO/UiO-66 is slightly higher than that of $H_2$/UiO-66. The proximity of the adsorption heat for two systems indicates that the adsorption process is the same in them, because the hydrophobicity is very high while the load is very low. The reason for the low adsorption heat can be related to the low amount of the adsorbents. At the low loads, the A-A interactions are not significant, and consequently, less isosteric heat is obtained for the $H_2$/UiO-66 system.

### 3.5. Determination of diffusion coefficient

The diffusion coefficient for the diffuser was calculated by Einstein's relation:

$$D = \frac{1}{6N} \lim_{\to\infty} \frac{d}{dt} \sum_{t=1}^{N} < \left| r_i(t) - r_i(0) \right| >^2 \qquad (2)$$

in which N is the number of the diffusing atoms, $r_i$ is the atom location, $< \left| r_i(t) - r_i(0) \right|^2 >$ represents the MSD for the path of the entered molecular gas, and $r_i(t)$ and $r_i(0)$ are the vectors of the final and primary locations of the central mass of the gas molecules at the time t = t and t = 0, respectively. In addition, the diffusion coefficient of the self-correlation function of the computational speed is improved by the simulation software. The MSD gradient can be used as a function of time to estimate the diffusion coefficient [26]. To determine the permeability, the six molecules of each gas were added to the replication box by using the discovery module.

**Table 1.** The isosteric heat of the adsorbed H$_2$ and CO (q$_{H2}$ and q$_{CO}$, respectively) on the UiO-66 structure at the different temperatures.

| Temperature (K) | P (bar) | q$_{H2}$ (kJ/mol) | q$_{CO}$ (kJ/mol) |
|---|---|---|---|
| 273 | 1-3000 | 2.23 | 4.29 |
| 298 | 1-3000 | 2.22 | 4.27 |
| 313 | 1-3000 | 2.23 | 4.28 |
| 333 | 1-3000 | 2.23 | 4.20 |
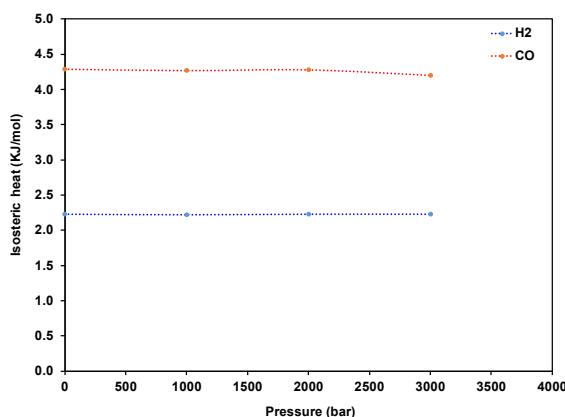


**Figure 4.** Isosteric heats for the H$_2$ and CO adsorption on the UiO-66 framework.
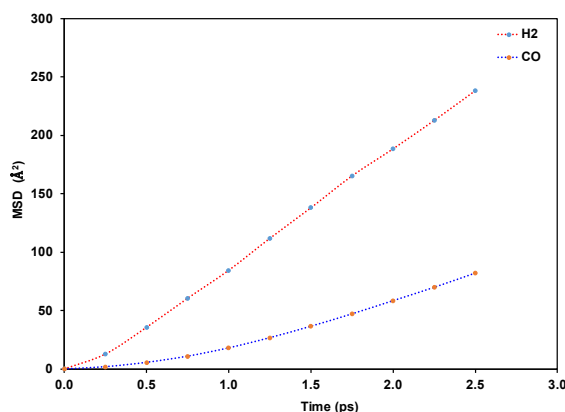


**Figure 5.** MSD plot of CO and H$_2$ adsorbed on the UiO-66 framework.

Before adding the gas molecules, the energy minimization step was performed on the gas molecules. MSDs were calculated from the paths of the gas molecules in each cell and used to obtain their diffusion coefficients. In a short time, the gas molecules are trapped into the small holes inside the free volume, and the level of MSD remains almost constant. In a long time, the molecules leave the confined region and move to another cavity of the free volume. The result of the repetition of these movements is the diffusion. The diffusion coefficient was calculated by using the Einstein's relation [26] and fitting to the straight line ($y$ = a$x$ + b). Figure 5 shows the MSD of the adsorbed H$_2$ and CO on UiO-66 at 273, 298, 313, and 333 K temperatures. Based on Figure 5, the displacement increases with increasing time (for a constant load of 8 molecules per unit cell). The self-penetration coefficients indicate that the H$_2$ penetration to the base of UiO-66 possesses a different behavior compared to CO. The electrostatic interaction of CO with UiO-66 prevents it to penetrate and move further in the other parts of the structure.

One of the effective parameters on the penetration of a molecule to a porous structure is its molecular mass, described by Graham's law (Equation 3).

$$r\alpha = \frac{1}{\sqrt{M}} \tag{3}$$

in which r and M parameters are the gas accumulation and molar mass of gas, respectively. According to Graham's law, the rate of the gas diffusion depends on its molecular weight [27]. In fact, the gases with less molecular weight pass through the cavity faster than those with more weight. A gas with a lower molecular weight has a higher penetration rate and a shorter penetration time. The penetration coefficient is calculated by considering the slope of the MSD diagram over time, reported in Table 2. The magnitude of the diffusion coefficient for H$_2$ is greater than that of CO. To highlight the effect of the molecular size on the diffusion coefficient, the Van der Waals volumes are calculated and given in Table 3. The gas molecule with smaller volume is expected to have a higher diffusion coefficient; however, it is vice versa in the case of the studied molecules. CO molecule is smaller in volume than H$_2$, but the diffusion coefficient of the latter is higher. The kinetic diameter as another impressive factor greatly affects the diffusion coefficient.

The kinetic diameter is dependent on the geometry of the molecule. The denser and more compact structure of the electron cloud around the nucleus of CO and stronger electrostatic interaction between the negatively charged electrons and positively charged atoms in CO molecule induce a greater kinetic diameter of CO molecule in comparison with H$_2$. Hence, the penetration coefficient in CO is smaller than that of H$_2$ molecule.

**Table 2.** Diffusion coefficient of the gas molecules.

| Gas | T (°C) | D×10⁻⁹ (m²/S) |
|---|---|---|
| $H_2$ | 273 | 4 |
|  | 298 | 5 |
|  | 313 | 7 |
|  | 333 | 15 |
| CO | 273 | 2 |
|  | 298 | 3 |
|  | 313 | 4 |
|  | 333 | 8 |

**Table 3.** Molecular size of the gas molecules.

| Gas | Volume (Å³) | Kinetic diameter (Å) |
|---|---|---|
| $H_2$ | 46.23 | 0.28 |
| CO | 33.60 | 0.32 |

## 4. Conclusion

In this study, the adsorption of $H_2$ and CO on the UiO-66 framework is examined by using Monte Carlo simulation. The simulations are performed for studying the penetration of the gas molecules, showing that the increase in the temperature is associated with an enhancement of the gas penetration. In addition, the results show that the volume of the structure has no effect on the penetration process in the studied systems. The diffusion coefficient is affected by the type of the penetrating molecule. According to Graham's molecule law, $H_2$ molecule greatly moves into the UiO-66 structure, due to its less mass. The Monte Carlo results highlight that the addition of $H_2$ to the UiO-66 structure increases the absorption capacity. The amount of adsorbed gas molecules on UiO-66 decreases with the enhancement of the temperature and increases at the high pressures. The adsorption isotherms for the studied systems follow Langmuir model isotherm.

## Acknowledgement

## Disclosure statement DS

Conflict of interests: The authors declare that they have no conflict of interest.
Author contributions: All authors contributed equally to this work.
Ethical approval: All ethical guidelines have been adhered.
Sample availability: Samples of the compounds are available from the author.

## ORCID iD

Negin Davoodian
iD http://orcid.org/0000-0001-8995-609X
Zahra Khoshbin
iD http://orcid.org/0000-0002-6939-2036

## References

[1]. Sun, X.; Li, J.; Qiao, H.; Zhang, B. *Appl. Energy* **2017**, *196*, 118-131.
[2]. Niakolas, D. K.; Daletou, M.; Neophytides, S. G.; Vayenas, C. G. *Ambio*. **2016**, *45(1)*, 32-37.
[3]. Das, V.; Padmanaban, S.; Venkitusamy, K.; Selvamuthukumaran, R.; Blaabjerg, F.; Siano, P. *Renew. Sust. Energ. Rev.* **2017**, *73*, 10-18.
[4]. Gilman, S. *J. Phys. Chem.* **1963**, *67(1)*, 78-84.
[5]. Shadman, M.; Yeganegi, S.; Galugahi, M. R. *J. Iranian Chem. Soc.* **2016**, *13(2)*, 207-220.
[6]. Tian, Z.; Dong, S. *Inter. J. Hydrog. Energy* **2016**, *41(2)*, 1053-1059.
[7]. Zhang, W.; Zhang, Z.; Zhang, F.; Yang, W. *Appl. Surf. Sci.* **2016**, 386, 247-254.
[8]. Yang, S.; Lin, X.; Dailly, A.; Blake, A. J.; Hubberstey, P.; Champness, N. R.; Schroder, M. *Chem. Eur. J.* **2009**, *15(19)*, 4829-4835.
[9]. Gomez, D. A.; Sastre, G. *Phys. Chem. Chem. Phys.* **2011**, *13(37)*, 16558-16568.
[10]. Zhang, F. M.; Sheng, J. L.; Yang, Z. D.; Sun, X. J.; Tang, H. L.; Lu, M.; Lan, Y. Q. *Angew. Chem. Inter.* **2018**, *57(37)*, 12106-12110.
[11]. Li, J. R.; Ma, Y.; McCarthy, M. C.; Sculley, J.; Yu, J.; Jeong, H. K.; Zhou, H. C. *Coord. Chem. Rev.* **2011**, *255(15-16)*, 1791-1823.
[12]. Rowsell, J. L.; Spencer, E. C.; Eckert, J.; Howard, J. A.; Yaghi, O. M. *Science* **2005**, *309(5739)*, 1350-1354.
[13]. Thommes, M.; Kaneko, K.; Neimark, A. V.; Olivier, J. P.; Rodriguez-Reinoso, F.; Rouquerol, J.; Sing, K. S. *Pure Appl. Chem.* **2015**, *87(9-10)*, 1051-1069.
[14]. Yang, Z.; Xia, Y.; Sun, X.; Mokaya, R. *J. Phys. Chem. B* **2006**, *110(37)*, 18424-18431.
[15]. Xie, H.; Shen, Y.; Zhou, G.; Chen, S.; Song, Y.; Ren, J. *Mater. Chem. Phys.* **2013**, *141(1)*, 203-207.
[16]. Greathouse, J. A.; Allendorf, M. D. *J. Am. Chem. Soc.* **2016**, *128(33)*, 10678-10679.
[17]. Zheng, B.; Yun, R.; Bai, J.; Lu, Z.; Du, L.; Li, Y. *Inorg. Chem.* **2013**, *52(6)*, 2823-2829.
[18]. Belof, J. L.; Stern, A. C.; Eddaoudi, M.; Space, B. *J. Am. Chem. Soc.* **2007**, *129(49)*, 15202-15210.
[19]. Colon, Y. J.; Brand, S. K.; Snurr, R. Q. *Chem. Phys. Lett.* **2013**, *577*, 76-81.
[20]. Yang, Q.; Zhong, C. *J. Phys. Chem. B* **2005**, *109(24)*, 11862-11864.
[21]. BIOVIA Materials Studio, Retrieved Aug 01, 2020, from https://www.3ds.com/products-services/biovia/products/molecular-modeling-simulation/biovia-materials-studio/
[22]. Valenzano, L.; Civalleri, B.; Chavan, S.; Bordiga, S.; Nilsen, M. H.; Jakobsen, S.; Lamberti, C. *Chem. Mater.* **2011**, *23(7)*, 1700-1718.
[23]. Fast, C. D.; Woods, J.; Lentchner, J.; Makal, T. A. *Dalton Trans.* **2019**, *48(39)*, 14696-14704.
[24]. Zhou, L.; Zhou, Y. *Inter. J. Hydrog. Energ.* **2001**, *26(6)*, 597-601.
[25]. Chen, C.; Chen, D.; Xie, S.; Quan, H.; Luo, X.; Guo, L. *ACS Appl. Mater. Interf.* **2017**, *9(46)*, 41043-41054.
[26]. Uneyama, T.; Miyaguchi, T.; Akimoto, T. *Phys. Rev. E* **2015**, *92(3)*, 032140.
[27]. Solcova, O.; Snajdaufova, H.; Schneider, P. *Chem. Eng. Sci.* **2001**, *56(17)*, 5231-5237.